Journal of Power Sources 209 (2012) 278–281

Contents lists available at SciVerse ScienceDirect

Journal of Power Sources

journal homepage: www.elsevier.com/locate/jpowsour

Short communication

Ionic distribution and conductivity in lithium garnet $Li_7La_3Zr_2O_{12}$

Yutao Li[a,b], Jian- Tao Han[c], Chang- An Wang[a], Sven C. Vogel[c], Hui Xie[b], Maowen Xu[b], John B. Goodenough[b,*]

[a] State Key Laboratory of New Ceramics and Fine Processing, Department of Materials Science and Engineering, Tsinghua University, Beijing 100084, PR China
[b] Materials Research Program and the Texas Materials Institute, ETC9.184, University of Texas at Austin, TX 78712, United States
[c] Los Alamos National Laboratory, Lujan Center. Mail Stop H805, Los Alamos, NM 87545, United States

ARTICLE INFO

Article history:
Received 31 October 2011
Received in revised form 23 February 2012
Accepted 26 February 2012
Available online 6 March 2012

Keywords:
Li^+-ion solid electrolyte
Li garnet
$Li_7La_3Zr_2O_{12}$
Lithium ion battery

ABSTRACT

The garnet-related oxide with nominal formula $Li_7La_3Zr_2O_{12}$ prepared by the sol–gel method is cubic, space group *Ia-3d* with lattice parameter $a = 12.9720$ Å at room temperature. The occupancies of three lithium positions (24*d*, 48*g*, 96*h*) and the position of a small amount of Al^{3+} (ca 0.61 wt%) inside the grains were determined by neutron diffraction. The occupancy of the 24*d* Li sites was reduced to 36.0% by the Al^{3+} occupying the 48*g* sites. The bulk and total Li^+-ion conductivity at 25 °C was 3.1×10^{-4} S cm^{-1} and 1.4×10^{-4} S cm^{-1} with an activation energy 0.34 eV in the temperature range 25–160 °C.

1. Introduction

A Li^+-ion solid electrolyte with a Li^+-ion conductivity $\sigma_{Li} > 10^{-4}$ S cm^{-1} and with a lowest unoccupied molecular orbital (LUMO) above the Fermi energy of Lithium (the Li^+/Li^0 energy) and a highest occupied molecular orbital at least 4.0 eV below Li^+/Li^0 would allow use of lithium as the anode and exploration of cathodes that are not insertion compounds [1]. A solid Li^+-ion electrolyte as separator or supported by the anode current collector would, if stable on contact with Lithium, allow use of lithium as the anode. If the electrolyte is to separate a lithium anode and an aqueous, flow-through cathode, the solid electrolyte must be an oxide.

Earlier searches for a suitable Li^+-ion solid electrolyte have identified the following candidates: Li_3N [2], the glass–ceramic system (Li_2O–Al_2O_3–TiO_2–P_2O_5)[3], LISICON ($Li_{2+2x}Zn_{1-x}GeO_4$)[4], $LiZr_{2-x}Ti_x(PO_4)_3$ with the NASICON structure [5], and the perovskite $Li_{0.29}La_{0.57}TiO_3$ ($0 < x < 0.16$)[6–8]. The top of the N-2p bands of Li_3N has too high an energy to allow a cathode with a competitive voltage and the other oxides identified are all unstable on contact with lithium. For example, the system $Li_{3x}La_{2/3-x}TiO_3$ ($0 < x < 0.16$)[9,10] exhibits a $\sigma_{Li} \approx 10^{-3}$ S cm^{-1} at room temperature, but Ti(IV) is reduced to Ti(III) on contact with lithium.

Recently, Li-rich oxides with garnet structure have been studied extensively for potential use in electrochemical applications due to the observation of a room-temperature Li^+-ion conductivity $\sigma_{Li} > 10^{-4}$ S cm^{-1} at 25 °C in a nominal "$Li_7La_3Zr_2O_{12}$" [16]. In the garnet structure $A_3B_3C_2O_{12}$, the $B_3C_2O_{12}$ framework contains a 3D-connected interstitial space of tetrahedral A sites 24*d* that are bridged by empty face-sharing octahedral sites 48*g*. In $Li_xB_3C_2O_{12}$ compounds with $x > 3$, the Li^+–Li^+ interaction across a shared 24*d*-48*g* face displaces the Li^+ in the bridging octahedral site to a position 96*h* near the opposite face, which requires that the 24*d* site sharing the opposite face be empty. In order to optimize σ_{Li}, a variety of garnet-related compounds $Li_{5+x}A_xLa_{3-x}M_2O_{12}$ (A = Ca, Sr, Ba; M = Nb, Ta)[11–15] as well as "$Li_7La_3Zr_2O_{12}$" [16–19] have been investigated. The "$Li_7La_3Zr_2O_{12}$" compound contained an undetermined amount of adventitious Al^{3+} because of its preparation at high temperature in an alumina crucible. Stability on contact with lithium and a room-temperature $\sigma_{Li} > 10^{-4}$ S cm^{-1} appeared to make "$Li_7La_3Zr_2O_{12}$" the best candidate with regard to safety for a rechargable high-energy-density battery.

In a previous work, we reported that a cubic aluminum-free $Li_7La_3Zr_2O_{12}$ prepared at 750 °C gave a $\sigma_{Li} \approx 10^{-6}$ S cm^{-1} and decomposed on heating above 800 °C [20]. From this observation and a neutron-diffraction study of the sample, we deduced that $x = 7.5$ is the upper limit of x that can be tolerated in a $Li_xB_3C_2O_{12}$ garnet framework and that this ideal limit requires 0.5 long-range ordered vacancies in the tetrahedral 24*d* sites. However, the distribution of the Al^{3+} ions inside the grains versus those acting as a sintering agent by residing in the grain boundaries has not previously been determined.

* Corresponding author at: Materials Research Program and the Texas Materials Institute, ETC9.184, University of Texas at Austin, TX 78712, United States.
Tel.: +1 512 471 1646; fax: +1 512 471 7681.
E-mail address: jgoodenough@mail.utexas.edu (J.B. Goodenough).

0378-7753/$ – see front matter © 2012 Elsevier B.V. All rights reserved.
doi:10.1016/j.jpowsour.2012.02.100

Here we report the synthesis of "$Li_7La_3Zr_2O_{12}$" by a new sol–gel method. Powder Electron Dispersive Spectroscopy (EDS), inductively coupled plasma-optical emission spectroscopy (ICP-OES), X-ray diffraction (XRD) and AC impedance spectroscopy were used to determine element distribution, phase formation, and the Li^+-ion conductivity. The distribution of lithium and aluminum were determined by neutron diffraction.

2. Experimental

Lithium nitrate, lanthanum nitrate, Zirconium (IV) n-propoxide, 200 proof anhydrous ethanol and hydroxypropyl cellulose polymer (molecular weight 100,000) were used as the starting materials to prepare the "$Li_7La_3Zr_2O_{12}$" solid electrolyte. The molar ratio of $LiNO_3$:$La(NO_3)_3$:$ZrC_{12}H_{28}O_4$ was 7.7:3:2; 10 wt% excess of $LiNO_3$ was added to compensate for lithium loss during heat treatment.

During synthesis, two different, but equal parts of alcohol solutions were prepared. In the first part, deionized water, $LiNO_3$ and $La(NO_3)_3$ were dissolved into anhydrous ethanol in a specific proportion; an appropriate amount of hydroxypropyl cellulose polymer was then added and dissolved completely by stirring the solution for 12 h with a magnetic stirrer. The second part of the alcohol solution was prepared by dissolving a specific amount of $ZrC_{12}H_{28}O_4$ in anhydrous ethanol under atmospheric conditions. Hydrolysis of $ZrC_{12}H_{28}O_4$ was carried out by rapidly mixing the two solutions under vigorous stirring. The sol was stirred slowly for 4 h and subsequently dried at 80 °C for 24 h to remove the solvent completely. The obtained gel was heated to 900 °C to decompose the metal salts. The powders were ground and sintered at 1125 °C for 6 h. Finally the powders were ground again and pressed into a pellet under 40 MPa and then annealed at 1200 °C for 36 h in air while the pellet was covered with the same mother powder.

Powder X-ray diffraction (Philips PW1830, Cu Kα) was employed to monitor the phase formation in the 2-theta range from 10 to 70° with a step size of 0.02°. A field-emission scanning electron microscope (Quanta FEG650) with an EDS attachment was used to obtain the fracture-surface microstructure of the pellet and the element distribution. The composition distribution of the elements was also measured with inductively coupled plasma-optical emission spectroscopy (ICP-OES).

Neutron diffraction experiments were conducted on the high-pressure preferred orientation neutron diffractometer (HIPPO) at the Lujan Neutron Scattering Center, Los Alamos National Laboratory. Bulk samples were placed in a vanadium holder and time-of-flight data were collected under vacuum at room temperature. Neutrons were detected with 27 detector panels of ^3He detector tubes arranged on three rings with nominal diffraction angles of 40°, 90°, and 144°.

Ionic conductivity was measured from 288 to 425 K with a Solar impedance Analyzer (Model 1287); the applied frequency range was from 10^6 to 1 Hz with a 10 mV AC amplitude. Both parallel surfaces of the pellet were sputtered with Li^+-ion-blocking Au electrodes.

3. Results and discussion

Fig. 1 shows the powder XRD patterns after each heat treatment together with the standard pattern of $Li_5La_3Nb_2O_{12}$. At 900 °C, the "$Li_7La_3Zr_2O_{12}$" showed a tetragonal garnet structure that turned into a cubic phase after heat-treatment at 1200 °C for 36 h; the diffraction peaks observed after heat treatment were assigned to a well-crystallized garnet-related structure. Impurities such as pyrochlore $La_2Zr_2O_7$ were not found. The "$Li_7La_3Zr_2O_{12}$" crystallizes very well and no clear grain boundary can be observed (Fig. 1S). Isolated pores remain trapped in the bulk.

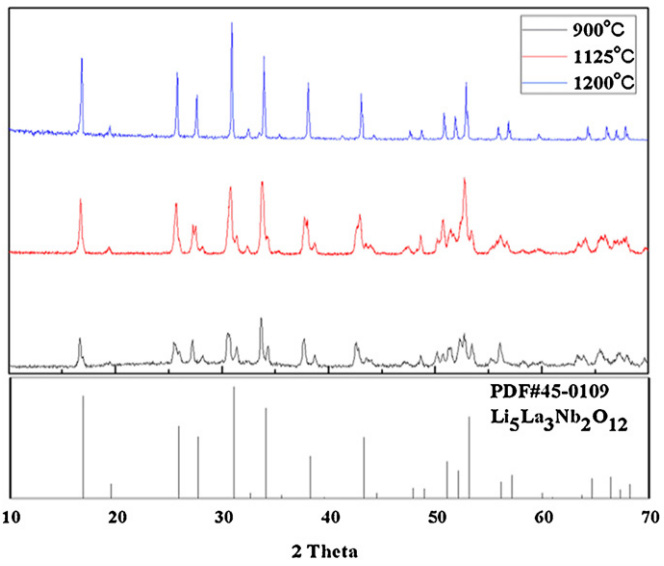

Fig. 1. Powder XRD results after sintering at different temperatures.

The structure of cubic $Li_5La_3Nb_2O_{12}$ in which the lithium was disordered with occupancies of 11% octahedral sites (48*g*), 15.2% displaced in octahedral sites (96*h*) and 83.6% tetrahedral sites (24*d*) was adopted as the initial structure model. Three lithium crystallographic sites and oxygen sites were refined. With these refinement conditions, the reliability factors converged quickly to satisfactory values. A fitted diffraction pattern is shown in Fig. 2S. The final Bragg-*R* factor (R = 3.38) indicated a good refinement. Our cubic garnet "$Li_7La_3Zr_2O_{12}$" had space group *Ia-3d* with lattice parameter a = 12.9720 Å at room temperature, which is a little smaller than the 12.9751 Å reported by Geigers and Lazic [18] and larger than the 12.9682 Å reported by Murugan et al. [16].

In order to identify the Li^+-ion and possible Al^{3+}-ion distribution inside the "$Li_7La_3Zr_2O_{12}$" grains, a room-temperautre neutron-diffraction pattern was collected. Li- atom coordinates and occupancies are listed in Table 1. The positions and occupancies of lithium, aluminum and oxygen sites were refined. The fit cannot converge by allowing a distribution of Al across both the tetrahedral (24*d*) and displaced octahedral (96*h*) sites; the refinement quality was improved by allowing Al in the octahedral (48*g*) site (R_p = 0.0105, R_{wp} = 0.017, χ^2 = 9.72) compared to the refinement without Al (R_p = 0.015, R_{wp} = 0.022, χ^2 = 10.20). The crystal structure of "$Li_7La_3Zr_2O_{12}$" and the fitted diffraction pattern are shown in Figs. 2 and 3, respectively; the final R_p and R_{wp} values show the refinement is good; 6.4 Li atoms could be located at three different sites; few oxygen-ion vacancies exist. The Li occupancies are 36.0% in the tetrahedral 24*d* site, 25.0% in the octahedral 48*g* site and 31.7% in the displaced octahedral 96*h* Li^+ site. The Debye–Waller parameters of the tetrahedral 24*d* and displaced octahedral 96*h* Li^+ site are higher than that of the octahedral 48*g* Li^+ site. The refinement only converged if the Al^{3+} occupy the octahedral 48*g* sites.

O'Callaghan and Cussen [21] have reported the correlation with x of the Li^+ site occupancies for the system $Li_{5+x}Ba_xLa_{3-x}Ta_2O_{12}(0 < x \leq 1.6)$. In our "$Li_7La_3Zr_2O_{12}$" sample, the occupancy of the tetrahedral 24*d* site is 36.0% compared to their $Li_{6.6}Ba_{1.6}La_{1.4}Ta_2O_{12}$ result (56.8%), while the occupancies of the octahedral 48*g* and displaced 96*h* sites do not change too much. A small amount of Al^{3+} (ca 0.61%) was found in the bridging octahedral 48*g* position, which is consistent with Coulomb repulsions repelling Li^+ from both neighboring tetrahedral sites. The 0.19 Al in the deduced formula "$Li_{6.4}Al_{0.19}La_3Zr_2O_{11.8}$", introduce 0.5 Li^+ vacancies per formula unit and reduce the Li^+ occupancy on the

Table 1
Structural parameters of $^{7}Li_7La_3Zr_2O_{12}$ garnet from Rietveld refinement of neutron diffraction data.

Atom	Site	*x*, *y*, *z*	Occupation	Uiso
Li1	*24d*	0.375, 0, 0.25	0.360(3)	0.0330(4)
Li2	*48g*	0.125, 0.6796(3), 0.5704(7)	0.250(4)	0.0149(7)
Li3	*96h*	0.0911(5), 0.1914(5), 0.4236(6)	0.317(4)	0.0201(1)
Al	*48g*	0.125, 0.6796(2), 0.5704(7)	0.032 (1)	0.0384(5)
La	*24c*	0.125, 0, 0.25	1	0.0072(4)
Zr	*16a*	0, 0, 0	1	0.0071(6)
O	*96h*	0.0999(7), 0.1963(3), 0.2817(4)	0.984(6)	0.0107(8)
$R_p/R_{wp}/CHI^2$	0.0105/0.0171/9.72			

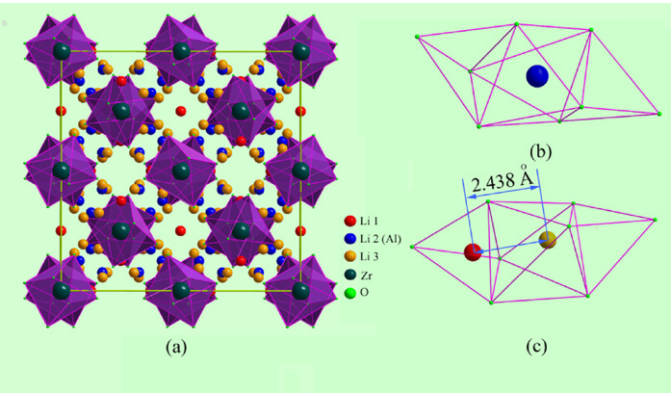

Fig. 2. (a) Crystal structure of cubic $Li_7La_3Zr_2O_{12}$ from neutron diffraction, see Table 1 for positions of atoms. (b) The 48*g* occupied requiring two empty neighboring 24*d* Li sites. (c) The 48*g* Li displaced to 96*h* with separation to 2.438 Å from the occupied 24*d* Li atom; the other neighboring Li site remains empty.

two neighboring tetrahedral 24*d* Li^+ sites. Nyman [22] has argued that the Li^+ ions in the tetrahedral 24*d* sites are preferentially vacated by Li_2O volatility upon repeated mixing and heating solid-state processing steps, which leads to a decreased activation energy for lithium mobility in $Li_{5-x}La_3Ta_2O_{12-x/2}$. Consequently, the Al^{3+} inside the "$Li_7La_3Zr_2O_{12}$" grains from a high-temperature firing in an alumina crucible and a high sintering temperature (1200 °C for 36 h) can result in largely different Li^+ distributions compared to those in other Li-rich garnet frameworks, especially in the tetrahedral 24*d* sites.

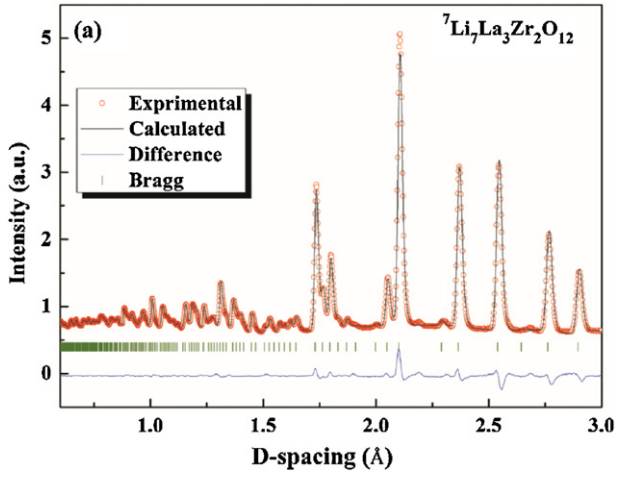

Fig. 3. Observed, calculated, and difference patterns for the Rietveld refinement from the neutron diffraction of cubic $Li_7La_3Zr_2O_{12}$. The short vertical lines below the profiles mark the peak positions of all possible Bragg reflections of cubic $Li_7La_3Zr_2O_{12}$.

Table 2 shows selected interatomic distances in the "$Li_7La_3Zr_2O_{12}$" garnet. The Li^+ ions occupy the 24*d* tetrahedral and distorted octahedral sites. The short Li^+–Li^+ contact (1.987 Å) between Li^+ on neighboring 24*d* and 48*g* sites introduce a Coulomb repulsion that displaces the octahedral-site Li^+ ions to a 96*h* site neighboring an empty 24*d* site to give a 2.438 Å Li^+–Li^+ separation; a Li^+ ion is not stable in a 48*g* site that bridges two occupied 24*d* sites at 1.987 Å. The larger charge on an Al^{3+} ion in a 48*g* site displaces Li^+ ions from both neighboring 24*d* sites.

The distribution of Al^{3+} obtained by EDS is shown in Fig. 3S; the Al element, which can originate from the alumina crucible at high temperature, is evenly distributed in the sample. The molar ratio of Al^{3+}:La^{3+}:Zr^{4+} obtained by EDS was 0.2:3:2.08. The ICP result showed the molar ratio of Li^+:Al^{3+}:La^{3+} was 6.2:0.3:2.85; EDS and ICP results indicate that the Al^{3+} in our "$Li_7La_3Zr_2O_{12}$" sample largely entered into the framework to reduce the Li^+ concentration and stablize the garnet structure. Geiger et al. [18] recently reported that about 1.1 wt% of Al^{3+} existed and occupied different Li sites in the garnet "$Li_7La_3Zr_2O_{12}$". The tetragonal "$Li_7La_3Zr_2O_{12}$" without Al transformed to cubic "$Li_7La_3Zr_2O_{12}$" between 100 and 150 °C while the Al-containing cubic "$Li_7La_3Zr_2O_{12}$" existed at room temperature [18]; Ying Jin [19] recently reported that 1.2 wt% added Al^{3+} can accelerate densification because of the existence of a liquid phase introduced by Al additions, but both a cubic and a tetragonal phase existed if 0.7 wt% was added at the same sintering procedure. We have suggested [23] that the role of Al^{3+} and it's concentration may depend on the Li^+ concentration in the garnet structure. For example, for $Li_6La_3ZrTaO_{12}$, the Al^{3+} appears to act primarily as a sintering aid in the grain boundries to provide a more dense ceramic as can be seen by comparison of the sample prepared in an alumina crucible and a zirconia crucible, while Al^{3+} in the "$Li_7La_3Zr_2O_{12}$" primarily enters the framework to stabilize the structure.

An impedance spectrum of the prepared "$Li_7La_3Zr_2O_{12}$" pellet measured at room temperature is exhibited in Fig. 4. The

Table 2
Selected interatomic distance (Å) in $^{7}Li_7La_3Zr_2O_{12}$ garnet from neutron diffraction.

La-O × 4	2.504(6)
La-O × 4	2.595(8)
Zr-O × 6	2.104(2)
Li1–O × 4	1.901(5)
Li2–O × 2	1.954(4)
Li2–O × 2	2.397(3)
Li2–O × 2	2.443(2)
Li3–O	1.842(7)
	2.033(7)
	2.186(1)
	2.224(4)
	2.680(5)
	2.789(9)
Li1–Li2	1.987(5)
Li1–Li3	2.438(9)

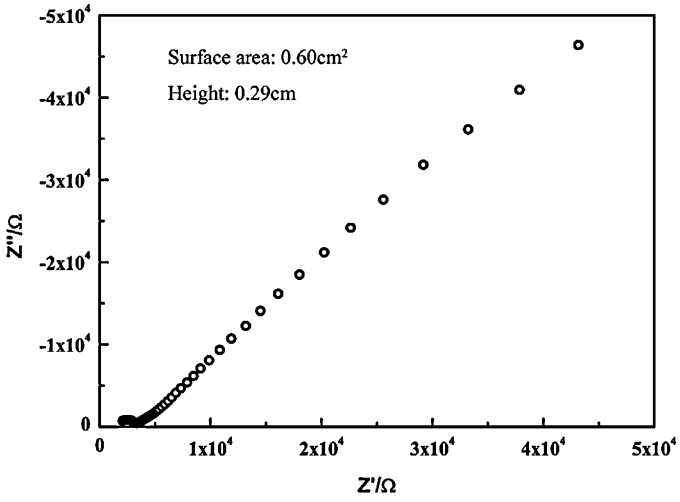

Fig. 4. Impedance plot (10 Hz–1 MHz) of $Li_7La_3Zr_2O_{12}$ measured in air after sintering at 1200 °C for 36 h at room temperature.

appearance of a low-frequency tail in the case of ionically blocking electrodes is an indication that the conductivity of "$Li_7La_3Zr_2O_{12}$" garnet is ionic in nature. A clear semicircle was observed in the high-frequency region, and the distance from zero to the intercept with the real axis at high and low frequency sides was assigned, respectively, to the bulk and total conductivity. The bulk and total lithium conductivity of "$Li_7La_3Zr_2O_{12}$" at room temperature is 3.1×10^{-4} and 1.4×10^{-4} S cm^{-1}, respectively.

Fig. 5 shows the lithium conductivity as a function of $1/T$ for a sintered sample of "$Li_7La_3Zr_2O_{12}$". The temperature dependence of the conductivity can be expressed by the Arrhenius equation.

$$\sigma T = A \exp\left(\frac{-E_a}{kT}\right)$$

where A is the pre-exponential factor, T is the absolute temperature, E_a is the activation energy and k is the Boltzmann constant. The activation energy was estimated to be $E_a = 0.34$ eV from the slope of the $\log \sigma T$ versus $1000/T$ plot in the temperature range of 300–400 K.

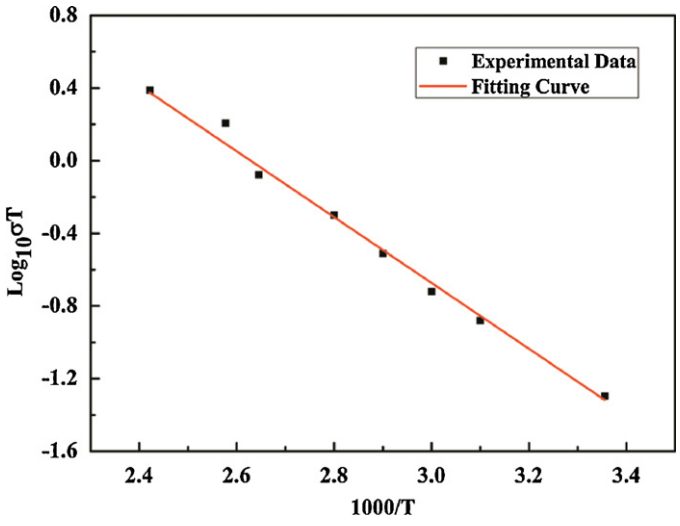

Fig. 5. Temperature dependence of lithium conductivity of $Li_7La_3Zr_2O_{12}$.

4. Conclusions

A cubic (s.g. *Ia-3d* and $a = 12.9720$ Å) garnet-related oxide "$Li_7La_3Zr_2O_{12}$" has been prepared by a sol–gel method and sintered at 1200 °C in an alumina crucible; it had a room-temperature Li^+-ion conductivity $\sigma_{Li(bulk)} \approx 3.1 \times 10^{-4}$ S cm^{-1} and $\sigma_{Li(total)} \approx 1.4 \times 10^{-4}$ S cm^{-1} with an activation energy 0.34 eV in the temperature range of 25–160 °C. The Li^+-ion distribution between three lithium positions (24*d*, 48*g*, 96*h*) and a small amount of Al^{3+} (ca. 0.61 wt%) were determined by neutron diffraction. 6.4 Li^+ per formula unit could be located at three different lithium positions and 0.19 Al^{3+} per formula unit occupy the 48*g* site in the framework. The Li^+ occupancy of the octahedral 48*g* and displaced 96*h* sites is 25.0% and 31.7%, respectively; the Al^{3+} inside the grains and high sintering temperature reduced the Li^+ occupancy of the tetrahedral sites to 36.0%, which makes "$Li_7La_3Zr_2O_{12}$" prepared by the sol–gel method described different from other Li rich garnet conductors. The adventitious Al^{3+}, which largely enters into the framework, creats more Li^+-ion vacancies and stabilizes the "$Li_7La_3Zr_2O_{12}$" structure.

Acknowledgment

Dr. Yutao Li thanks the China Scholarship Council for the opportunity to work in Texas. This work was supported by the Assistant Secretary for Energy Efficiency and Renewable Energy, Office of Vehicle Technologies, U.S. Department of Energy, under Contract DE-AC02-05CH11231 through the Batteries for Advanced Transportation Technologies (BATT) Program Subcontract 6805919.

Appendix A. Supplementary data

Supplementary data associated with this article can be found, in the online version, at doi:10.1016/j.jpowsour.2012.02.100.

References

[1] J.B. Goodenough, Y. Kim, Chemistry of Materials 22 (2010) 587–603.
[2] U.V. Alpen, A. Rabenau, G.H. Talat, Applied Physics Letters 30 (1977) 621–623.
[3] J. Fu, Solid State Ionics 96 (1997) 195–200.
[4] P.G. Bruce, A.R. West, Journal of the Electrochemical Society 130 (1983) 662–669.
[5] N.V. Kosova, E.T. Devyatkina, A.P. Stepanov, A.L. Buzlukov, Ionics 14 (2008) 303–311.
[6] P. Birke, S. Scharner, R.A. Huggins, W. Weppner, Journal of the Electrochemical Society 144 (1997) L167–L169.
[7] Y. Harada, H. Watanabe, J. Kuwano, Y. Saito, Journal of Power Sources 81 (1999) 777–781.
[8] K. Mizumoto, S. Hayashi, Solid State Ionics 127 (2000) 241–251.
[9] H. Aono, E. Sugimoto, Y. Sadaoka, N. Imanaka, G. Adachi, Chemistry Letters (1991) 1567–1570.
[10] S. Stramare, V. Thangadurai, W. Weppner, Chemistry of Materials 15 (2003) 3974–3990.
[11] V. Thangadurai, H. Kaack, W.J.F. Weppner, Journal of the American Ceramic Society 86 (2003) 437–440.
[12] B. Koch, M. Vogel, Solid State Nuclear Magnetic Resonance 34 (2008) 37–43.
[13] R. Murugan, W. Weppner, P. Schmid-Beurmann, V. Thangadurai, Materials Research Bulletin 43 (2008) 2579–2591.
[14] V. Thangadurai, W. Weppner, Journal of Power Sources 142 (2005) 339–344.
[15] R. Murugan, W. Weppner, P. Schmid-Beurmann, V. Thangadurai, Materials Science and Engineering B-Solid State Materials for Advanced Technology 143 (2007) 14–20.
[16] R. Murugan, V. Thangadurai, W. Weppner, Angewandte Chemie-International Edition 46 (2007) 7778–7781.
[17] M. Kotobuki, H. Munakata, K. Kanamura, Y. Sato, T. Yoshida, Journal of the Electrochemical Society 157 (2010) A1076–A1079.
[18] C.A. Geiger, E. Alekseev, B. Lazic, M. Fisch, T. Armbruster, R. Langner, M. Fechtelkord, N. Kim, T. Pettke, W. Weppner, Inorganic Chemistry 50 (2011) 1089–1097.
[19] Y. Jin, J. Paul, Mc. Ginn, Journal of Power Sources 196 (2011) 8683–8687.
[20] H. Xie, J.A. Alonso, Y. Li, M.T. Fernandez-Diaz, J.B. Goodenough, Chemistry of Materials 23 (16) (2011) 3587–3589.
[21] M.P. O'Callaghan, E.J. Cussen, Chemical Communications (2007) 2048–2050.
[22] M. Nyman, T.M. Alam, S.K. McIntyre, G.C. Bleier, D. Ingersoll, Chemistry of Materials 22 (2010) 5401–5410.
[23] Y. Li, C.-A. Wang, H. Xie, J. Cheng, J.B. Goodenough, Electrochemistry Communications 13 (12) (2011) 1289–1292.